Reconciling constraints from the supernova remnant HESS J1731-347 with the parity doublet model

Bikai Gao [1,*] Yan Yan [2,†] and Masayasu Harada [3,1,4,‡]

[1]*Department of Physics, Nagoya University, Nagoya 464-8602, Japan*

[2]*School of Microelectronics and Control Engineering, Changzhou University, Jiangsu 213164, China*

[3]*Kobayashi-Maskawa Institute for the Origin of Particles and the Universe, Nagoya University, Nagoya 464-8602, Japan*

[4]*Advanced Science Research Center, Japan Atomic Energy Agency, Tokai 319-1195, Japan*

(Received 9 April 2024; accepted 3 June 2024; published 24 June 2024)

The recent discovery of a central compact object (CCO) within the supernova remnant HESS J1731-347, characterized by a mass of approximately $0.77^{+0.20}_{-0.17}\ M_\odot$ and a radius of about $10.4^{+0.86}_{-0.78}$ km, has opened up a new window for the study of compact objects. This CCO is particularly intriguing because it is the lightest and smallest compact object ever observed, raising questions and challenging the existing theories. To account for this light compact star, a mean-field model within the framework of the parity doublet structure is applied to describe the hadron matter. Inside the model, part of the nucleon mass is associated with the chiral symmetry breaking while the other part is from the chiral invariant mass m_0 which is insensitive to the temperature and density. The value of m_0 affects the nuclear equation of state for uniform nuclear matter at low density and exhibits strong correlations with the radii of neutron stars. We point out that HESS J1731-347 can be explained as the lightest neutron star for $m_0 \simeq 850$ MeV.

DOI: 10.1103/PhysRevC.109.065807

I. INTRODUCTION

A neutron star (NS) is one of the most compact objects in the universe with a mass of 1–2 $M_\odot$ and a radius of $\approx$10 km. The NSs with extreme conditions provide us with a unique natural laboratory for investigating the phases of cold, dense matter, including the possibility of exotic states such as hyperons and even quarks appearing within these astrophysical objects. Understanding the properties of NSs requires information about its equation of state (EOS), which characterizes how pressure P varies as a function of the energy density ϵ. This EOS cannot be directly predicted by the quantum chromodynamics (QCD) and also the lattice QCD simulations due to the sign problem. Thanks to the advancements of recent multimessenger astronomy on different sources, especially those made by gravitational wave laser interferometers from the LIGO-VIRGO [1–3] and x-ray emissions observations conducted by the Neutron Star Interior Composition Explorer (NICER), we made remarkable improvements to constrain the EOS of cold, dense, and strongly interacting nuclear matter. For instance, the NS merger event GW170817 provided insights into the mass and the radius of NSs, with an estimation of approximately 1.4 $M_\odot$ and a radius of $R = 11.9^{+1.4}_{-1.4}$ km. This observation suggested that the EOS should be relatively soft for uniform nuclear matter existing in the low-density region. Additionally, NICER has played a crucial role in advancing our understandings of NSs. The analyses [4–6] have focused on NSs with masses around 1.4 and $\approx$2.1 $M_\odot$. Interestingly, the results indicated that the radii of these NSs are rather similar for different masses, with a radius of approximately 12.45 ± 0.65 km for a 1.4 $M_\odot$ NS and of 12.35 ± 0.75 km for a 2.08 $M_\odot$ NS. These findings suggest that the EOS stiffens rapidly, meaning that the pressure increases quickly as a function of energy density, as one moves from low baryon density ($\lesssim 2n_0$; n_0: nuclear saturation density) to high density ($4n_0$–$7n_0$). This stiffening of the EOS is necessary to support the existence of massive NSs, such as those with masses around 2 $M_\odot$.

The recent report on the central compact object (CCO) HESS J1731-347 [7], with an estimated mass and radius of the object of $M = 0.77^{+0.20}_{-0.17}\ M_\odot$ and $R = 10.4^{+0.86}_{-0.78}$ km, has raised many questions and put more constraints into the EOS. These measurements suggest that this CCO may correspond to a neutron star with an even softer equation of state in the low-density region than previously observed. Some studies have considered the possibility that HESS J1731-347 may be a quark star [8–12], an exotic theoretical object composed of deconfined quarks rather than the usual hadronic matter suggested in neutron stars.

In this research, we explore the possibility that HESS J1731-347 may be the neutron star within the framework of a quark-hadron crossover model constructed in Refs. [13–16], in which a unified EOS is constructed by interpolating the hadronic EOS from a hadronic model based on the parity doublet structure [17,18] and the quark EOS from an Nambu–Jona-Lasinio (NJL)-type quark model.

Hadronic models based on the parity doublet structure, which we call parity doublet models (PDMs), offer a unique perspective on the structure of hadrons by considering the

*Contact author: gaobikai@hken.phys.nagoya-u.ac.jp

†Contact author: 2919ywhhxh@163.com

‡Contact author: harada@hken.phys.nagoya-u.ac.jp

existence of the chiral invariant mass, denoted by m_0, in addition to the conventional chiral variant mass generated by the spontaneous chiral symmetry breaking. The existence of the chiral invariant mass is consistent with the lattice QCD simulation done at nonzero temperature [19–21]. The framework of PDMs has been widely used to study the hadron structure [22–27] and construct the EOS for nuclear and NS matter [13–16,28–49]. We note that the constructed EOS is softer for larger chiral invariant mass, and the resultant EOSs are combined with the EOS constructed from an NJL-type quark model by assuming quark-hadron crossover, which allows for a smooth transition from hadronic matter to quark matter [13–16,42,48]. This hybrid approach, where the PDM EOS is employed up to densities around $2n_0$–$3n_0$ and interpolates with the quark EOS at $\geqslant 5n_0$ via polynomial interpolation, is used to obtain the unified EOS. In this case, the unified EOS can be constructed with a soft EOS in the low-density part and a sufficiently stiff EOS in the high-density part to support the $2M_\odot$ constraint.

In this work, we consider a hadronic EOS constructed from a PDM in the low-density region and interpolate with quark EOS using an NJL-type quark model in the high-density region. Inside the PDM, we included the $\rho^2\omega^2$ interaction term with $\lambda_{\omega\rho}$ to be its coupling constant, which is assumed to make the EOS softer. By adjusting the two parameters $\lambda_{\omega\rho}$ and m_0, we can adjust the stiffness of the EOS in the hadronic model. The constructed unified EOS is shown to satisfy the constraints from HESS J1731-347 and makes it possible to be the lightest neutron star ever observed.

This paper is organized as follows. In Sec. II, we explain the formulation of the present model. The main results of the analysis of the properties of the NS are shown in Sec. III. Finally, we show the summary and discussions in Sec. IV.

II. EQUATION OF STATE

In this section, we briefly review how to construct the neutron star matter EOS from a PDM in the low-density region and from a NJL-type quark model in the high-density region.

A. Nuclear matter EOS

In Ref. [16], a hadronic PDM is constructed to describe the NS properties in the low-density region ($\leqslant 2n_0$). The model includes the effects of strange quark chiral condensate through the Kobayashi-Maskawa-'t Hooft (KMT)-type interaction in the mesonic sector. The density dependence of the strange quark chiral condensate $\langle\bar{s}s\rangle$ is calculated and the results show the impact of strange quark chiral condensate is very limited in the low-density region. Then, in the current study, we neglect the effect of strange quark in the low-density domain. In addition, we ignore the influence of the isovector scalar meson $a_0(980)$ in the current model, which is believed to appear in asymmetric matter like neutron stars. As investigated in Ref. [49], the effect of $a_0(980)$ has a negligible impact on the properties of neutron stars. Specifically, the inclusion of $a_0(980)$ only results in a slight increase in the radius by less than 1 km. We would like also to note that, in these analyses, a term of vector meson mixing, i.e., the $\omega^2\rho^2$ term, is introduced to make the slope parameter be consistent with the recent constraint shown in Ref. [50]. In the present analysis, we also include the mixing contribution.

TABLE I. Physical inputs in vacuum in units of MeV.

m_π	f_π	m_ω	m_ρ	m_+	m_-
140	92.4	783	776	939	1535

The thermodynamic potential is obtained as [14,43]

$$\begin{aligned}\Omega_{\rm PDM} &= V(\sigma) - V(\sigma_0) - \frac{1}{2}m_\omega^2\omega^2 - \frac{1}{2}m_\rho^2\rho^2 \\ &\quad - \lambda_{\omega\rho}(g_\omega\omega)^2(g_\rho\rho)^2 \\ &\quad - 2\sum_{i=+,-}\sum_{\alpha=p,n}\int^{k_f}\frac{{\rm d}^3\mathbf{p}}{(2\pi)^3}\left(\mu_\alpha^* - E_{\rm p}^i\right),\end{aligned} \tag{1}$$

where $i = +$ and $-$ denote the parity of nucleons and $E_{\mathbf{p}}^i = \sqrt{\mathbf{p}^2 + m_i^2}$ is the energy of nucleons with mass m_i and momentum $\mathbf{p}$. In Eq. (1), the potential $V(\sigma)$ is given by

$$V(\sigma) = -\tfrac{1}{2}\bar{\mu}^2\sigma^2 + \tfrac{1}{4}\lambda_4\sigma^4 - \tfrac{1}{6}\lambda_6\sigma^6 - m_\pi^2 f_\pi\sigma, \tag{2}$$

and σ_0 is the mean field at vacuum.

We note that the sign of λ is restricted to be positive due to the stability of the vacuum at zero density [49]. The total thermodynamic potential for the NS is obtained by including the effects of leptons as

$$\Omega_{\rm H} = \Omega_{\rm PDM} + \sum_{l=e,\mu}\Omega_l, \tag{3}$$

where Ω_l ($l = e$ and μ) are the thermodynamic potentials for leptons given by

$$\Omega_l = -2\int^{k_F}\frac{d^3\mathbf{p}}{(2\pi)^3}\left(\mu_l - E_{\mathbf{p}}^l\right). \tag{4}$$

The mean fields here are determined by following stationary conditions:

$$0 = \frac{\partial\Omega_{\rm H}}{\partial\sigma}, \quad 0 = \frac{\partial\Omega_{\rm H}}{\partial\omega}, \quad 0 = \frac{\partial\Omega_{\rm H}}{\partial\rho}. \tag{5}$$

We also need to consider the β equilibrium and the charge neutrality conditions,

$$\mu_e = \mu_\mu = -\mu_Q, \tag{6}$$

$$\frac{\partial\Omega_{\rm H}}{\partial\mu_Q} = n_p - n_l = 0, \tag{7}$$

where μ_Q is the charge chemical potential. We then have the pressure in hadronic matter as

$$P_{\rm H} = -\Omega_{\rm H}. \tag{8}$$

We then determine the parameters in the PDM by fitting them to the pion-decay constant and hadron masses given in Table I and the normal nuclear matter properties summarized in Table II for a fixed value of m_0. In addition, we use the slope parameter as an input to determine the coefficient $\lambda_{\omega\rho}$ of the ω-ρ mixing term. In the present analysis, we need to

TABLE II. Saturation properties used to determine the model parameters: the saturation density n_0, the binding energy B_0, the incompressibility K_0, and the symmetry energy S_0.

n_0 (fm^{-3})	$E_{\rm Bind}$ (MeV)	K_0 (MeV)	S_0 (MeV)
0.16	16	240	31

use the slope parameter as an input to determine the strength of the vector meson mixing (namely, the parameter $\lambda_{\rho\omega}$). The estimation in Ref. [50] provides the best value of $L = 57.7 \pm 19$ MeV.

For studying this sensitivity, we first study the EOSs for $L = 40$, 57.7, 70, and 80 MeV with $m_0 = 800$ MeV fixed.

In Table III, we summarize the values of the parameters $g_{\rho NN}$ and $\lambda_{\omega\rho}$ for several choices of the chiral invariant mass and the slope parameter.Since the introduction of ω-ρ mixing does not have an impact on the normal nuclear matter construction, the coupling constants of scalar mesons $\bar{\mu}^2$, λ_4, and λ_6 are exactly the same as those determined in Ref. [14], and we only list the values for $\lambda_{\omega\rho}$ and $g_{\rho NN}$.

The dependence on the slope parameter L for $m_0 = 800$ MeV is plotted in Fig. 1. This shows that the smaller L leads to a softer EOS as expected. As we show later, we need a very soft EOS in the low-density region to reproduce the HESS data. Then, we take $L = 40$ MeV as a typical choice in the preceding analysis.

We can then calculate the EOS in the hadronic model, and the corresponding EOS for the PDM with fixing the slope parameter $L = 40$ MeV is shown in Fig. 2. From this figure, we easily find that larger values of m_0 lead to softer EOSs. This is understood as follows: a greater m_0 leads to a weaker σ coupling to nucleons, because a nucleon does not have to acquire its mass entirely from the σ fields. The couplings to ω fields are also smaller because the repulsive contributions from ω fields must be balanced with attractive σ contributions

TABLE III. Determined values of $\lambda_{\omega\rho}$ and $g_{\rho NN}$ with different choices of the chiral invariant mass m_0 and the slope parameter L.

			$L = 40$ MeV		
m_0 (MeV)	500	600	700	800	900
$\lambda_{\omega\rho}$	0.045	0.087	0.192	0.504	3.243
$g_{\rho NN}$	7.31	7.85	8.13	8.30	8.43
			$L = 57.7$ MeV		
m_0 (MeV)	500	600	700	800	900
$\lambda_{\omega\rho}$	0.037	0.066	0.141	0.362	2.28
$g_{\rho NN}$	7.31	7.85	8.13	8.30	8.43
			$L = 70$ MeV		
m_0 (MeV)	500	600	700	800	900
$\lambda_{\omega\rho}$	0.028	0.045	0.088	0.211	1.252
$g_{\rho NN}$	7.31	7.85	8.13	8.30	8.43
			$L = 80$ MeV		
m_0 (MeV)	500	600	700	800	900
$\lambda_{\omega\rho}$	0.020	0.021	0.025	0.030	0.013
$g_{\rho NN}$	7.31	7.85	8.13	8.30	8.43

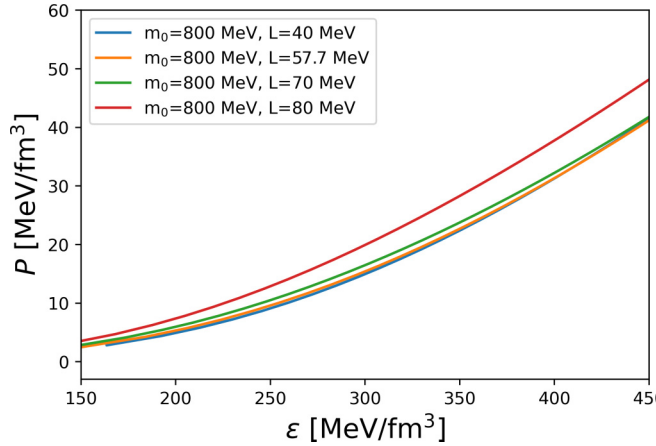

FIG. 1. EOS for different values of the slope parameter L for $m_0 = 800$ MeV.

at the saturation density n_0. At densities larger than n_0, however, the σ field reduces but the ω field increases, and these contributions are no longer balanced, affecting the stiffness of the EOS.

B. Quark matter EOS

Following Refs. [13,51], we use an NJL-type quark model to describe the quark matter. The model includes three-flavors and the U(1)$_A$ anomaly effects through the quark version of the KMT interaction. The coupling constants are chosen to be the Hatsuda-Kunihiro parameters which successfully reproduce the hadron phenomenology at low energy [13,52]: $G\Lambda^2 = 1.835$ and $K\Lambda^5 = 9.29$, with $\Lambda = 631.4$ MeV, see the definition below. The couplings g_V and H characterize the strength of the vector repulsion and the attractive diquark correlations whose range is examined later when we discuss the NS constraints.

We can then write down the thermodynamic potential as

$$\Omega_{\rm CSC} = \Omega_s - \Omega_s\big[\sigma_f = \sigma_f^0, d_j = 0, \mu_q = 0\big] + \Omega_c - \Omega_c\big[\sigma_f = \sigma_f^0, d_j = 0\big], \tag{9}$$

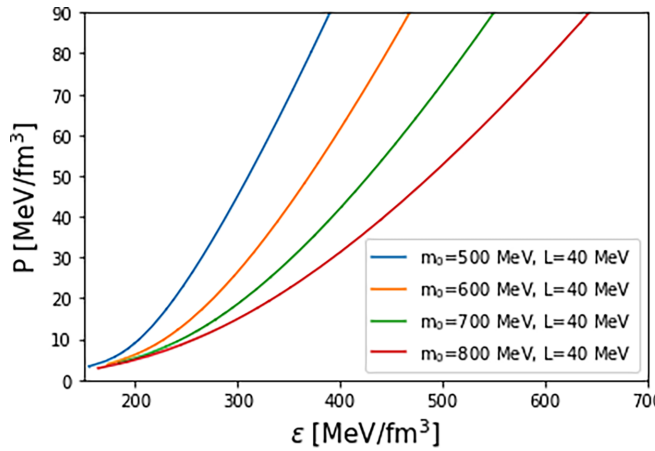

FIG. 2. EOS for different values of m_0 for $L = 40$ MeV.

where the subscript 0 is attached for the vacuum values, and

$$\Omega_s = -2\sum_{i=1}^{18}\int^{\Lambda}\frac{d^3\mathbf{p}}{(2\pi)^3}\frac{\epsilon_i}{2}, \tag{10}$$

$$\Omega_c = \sum_i \left(2G\sigma_i^2 + Hd_i^2\right) - 4K\sigma_u\sigma_d\sigma_s - g_V n_q^2, \tag{11}$$

where σ_f denotes the chiral condensates, d_j denotes the diquark condensates, and n_q denotes the quark density. In Eq. (10), ϵ_i are the energy eigenvalues obtained from the inverse propagator in the Nambu-Gorkov bases

$$S^{-1}(k) = \begin{pmatrix} \gamma_\mu k^\mu - \hat{M} + \gamma^0\hat{\mu} & \gamma_5\sum_i \Delta_i R_i \\ -\gamma_5\sum_i \Delta_i^* R_i & \gamma_\mu k^\mu - \hat{M} - \gamma^0\hat{\mu} \end{pmatrix}, \tag{12}$$

where

$$\begin{aligned} M_i &= m_i - 4G\sigma_i + K|\epsilon_{ijk}|\sigma_j\sigma_k, \\ \Delta_i &= -2Hd_i, \\ \hat{\mu} &= \mu_q - 2g_V n_q + \mu_3\lambda_3 + \mu_8\lambda_8 + \mu_Q Q, \\ (R_1, R_2, R_3) &= (\tau_7\lambda_7, \tau_5\lambda_5, \tau_2\lambda_2). \end{aligned} \tag{13}$$

$S^{-1}(k)$ is a 72×72 matrix in terms of the color, flavor, spin, and Nambu-Gorkov basis, which has 72 eigenvalues. $M_{u,d,s}$ are the constituent masses of u, d, and s quarks and $\Delta_{1,2,3}$ are the gap energies. $\mu_{3,8}$ are the color chemical potentials which are tuned to achieve the color neutrality. The total thermodynamic potential including the effect of leptons is

$$\Omega_{\rm Q} = \Omega_{\rm CSC} + \sum_{l=e,\mu}\Omega_l. \tag{14}$$

The mean fields are determined from the gap equations,

$$0 = \frac{\partial\Omega_{\rm Q}}{\partial\sigma_i} = \frac{\partial\Omega_{\rm Q}}{\partial d_i}, \tag{15}$$

From the conditions for electromagnetic charge neutrality and color charge neutrality, we have

$$n_j = -\frac{\partial\Omega_{\rm Q}}{\partial\mu_j} = 0, \tag{16}$$

where $j = 3$, 8, and Q. The baryon number density n_B is determined as

$$n_q = -\frac{\partial\Omega_{\rm Q}}{\partial\mu_q}, \tag{17}$$

where μ_q is 1/3 of the baryon number chemical potential. After determining all the values, we obtain the pressure as

$$P_{\rm Q} = -\Omega_{\rm Q}. \tag{18}$$

III. STUDY OF PROPERTIES OF NS

In this section, following Ref. [14] we construct a unified EOS by connecting the EOS obtained in the PDM introduced in Sec. II A and the EOS of the NJL-type quark model given in Sec. II B, and we solve the Tolman-Oppenheimer-Volkoff (TOV) equation [53,54] to obtain the NS mass-radius (M-R) relation. As for the interplay between nuclear and quark matter EOSs, see, e.g., Ref. [55] for a quick review that classifies types of the interplay.

TABLE IV. Unified EOS composed of four parts.

$0 \leqslant n_B < 0.5n_0$	$0.5n_0 \leqslant n_B \leqslant 2n_0$	$2n_0 < n_B < 5n_0$	$n_B \geqslant 5n_0$
Crust	PDM	Interpolation	NJL

A. Construction of unified EOS

In our unified equations of state as in Table IV, we use the (Baym-Pethick-Sutherland) EOS [56] as a crust EOS for $n_B \lesssim 0.5n_0$. From $n_B \simeq 0.5n_0$ to $2n_0$ we use our PDM model to describe nuclear matter. We limit the use of our PDM up to $2n_0$ so that baryons other than ground-state nucleons, such as the negative-parity nucleons or hyperons, do not show up in matter. Beyond the $2n_0$ nuclear regime, we assume a crossover from the nuclear matter to the quark matter, and we use a smooth interpolation to construct the unified EOS. We expand the pressure as a fifth-order polynomial of μ_B as

$$P_{\rm I}(\mu_B) = \sum_{i=0}^{5} C_i\mu_B^i, \tag{19}$$

where C_i ($i = 0, \ldots, 5$) are parameters to be determined from boundary conditions given by

$$\begin{aligned} \left.\frac{{\rm d}^n P_{\rm I}}{({\rm d}\mu_B)^n}\right|_{\mu_{BL}} &= \left.\frac{{\rm d}^n P_{\rm H}}{({\rm d}\mu_B)^n}\right|_{\mu_{BL}}, \\ \left.\frac{{\rm d}^n P_{\rm I}}{({\rm d}\mu_B)^n}\right|_{\mu_{BU}} &= \left.\frac{{\rm d}^n P_{\rm Q}}{({\rm d}\mu_B)^n}\right|_{\mu_{BU}}, \quad (n = 0, 1, 2), \end{aligned} \tag{20}$$

with μ_{BL} being the chemical potential corresponding to $n_B = 2n_0$ and μ_{BU} to $n_B = 5n_0$. We demand the matching up to the second-order derivatives of pressure at each boundary. The resultant interpolated EOS must satisfy the thermodynamic stability condition,

$$\chi_B = \frac{\partial^2 P}{(\partial\mu_B)^2} \geqslant 0, \tag{21}$$

and the causality condition,

$$c_s^2 = \frac{{\rm d}P}{{\rm d}\varepsilon} = \frac{n_B}{\mu_B\chi_B} \leqslant 1, \tag{22}$$

which means that the sound velocity is smaller than the light velocity. These conditions restrict the range of quark model parameters (g_V, H) for a given nuclear EOS and a choice of (n_L, n_U). We exclude interpolated EOSs which do not satisfy the abovementioned constraints. We note that the interpolation between the hadronic (PDM) and quark (NJL) models is performed over a relatively wide density range ($2n_0$–$5n_0$) because there is still significant uncertainty regarding the exact density at which the transition from hadronic to quark matter occurs in neutron stars. By choosing a broad interpolation range, we aim to capture a variety of possible transition scenarios.

B. Mass-radius relation

In this section, we calculate mass-radius relation of NSs by using the unified EOS constructed in the previous section for the PDM with different parameter choices of the chiral invariant mass m_0 and the slope parameter L.

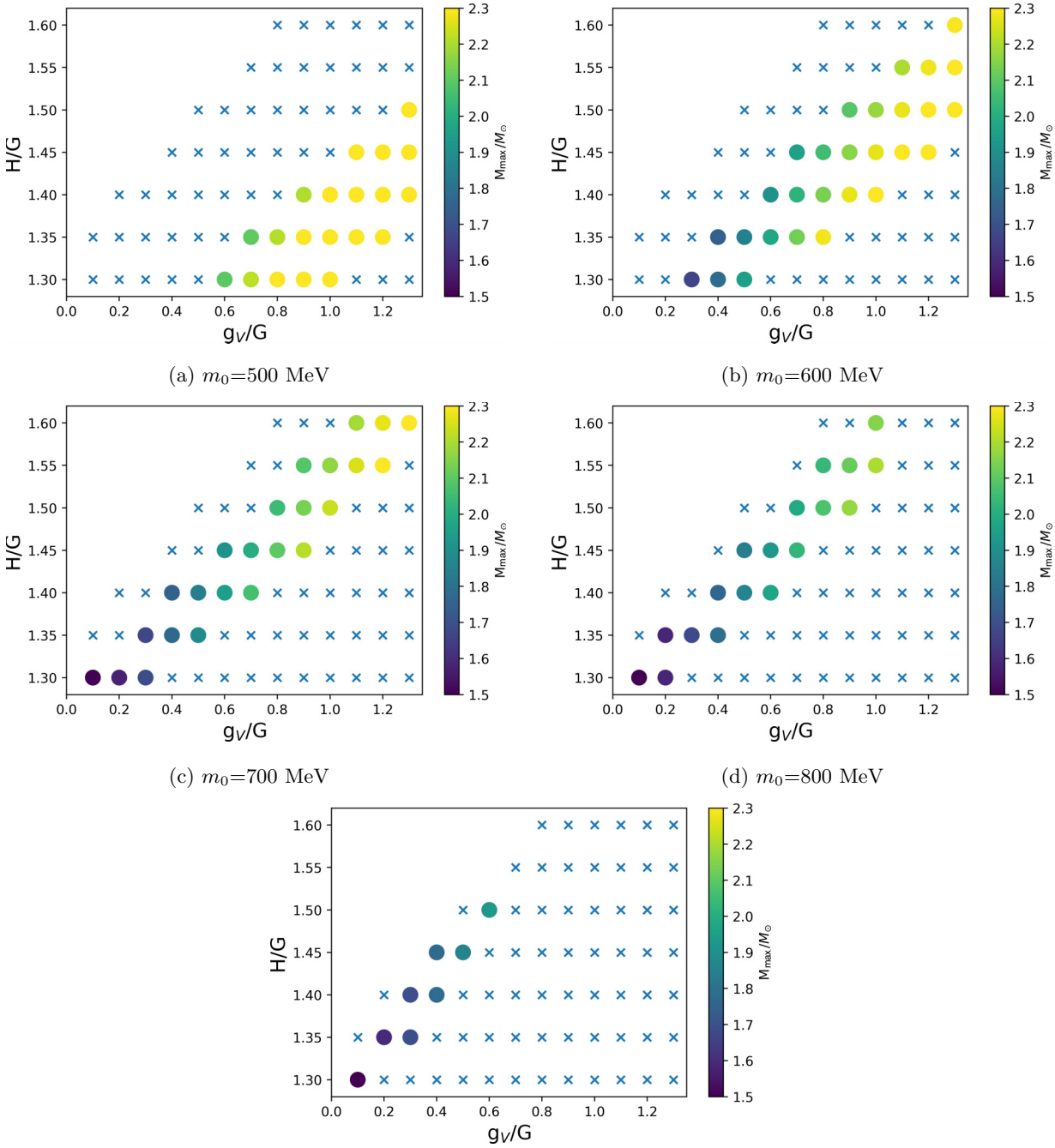

(a) m_0=500 MeV

(b) m_0=600 MeV

(c) m_0=700 MeV

(d) m_0=800 MeV

(e) m_0=900 MeV

FIG. 3. Allowed combination of (H, g_V) values for $m_0 = 500$, 600, 700, 800, and 900 MeV when $L = 40$ MeV. A cross mark indicates that the combination of (H, g_V) is excluded by the causality constraints. A circle indicates that the combination is allowed. The color shows the maximum mass of NS obtained from the corresponding parameters, as indicated by a vertical bar at the right side of each figure.

First, we study whether the smooth connection is realized depending on the parameters H and g_V in the NJL-type quark model as shown in Fig. 3 for PDM with $L = 40$ MeV. For each combination of (H, g_V), the cross marks are the parameter choices forbidden by the causality and thermodynamic stability conditions. For possible choices of (H, g_V), we determine the maximum mass of a NS, which is indicated by the color in Fig. 3. This shows that a larger g_V or/and a smaller H leads to a larger maximum mass. For $m_0 = 900$ MeV, the maximum mass for all the choices of (H, g_V) are below $2\,M_\odot$, leading to the conclusion that $m_0 = 900$ should be excluded when the slope parameter is chosen to be $L = 40$ MeV. In Fig. 4, we fix the value of m_0 with different choices of L and calculate the corresponding mass-radius curves, where the values of (H, g_V) are chosen to have the stiffest EOS. In this figure, the thick part indicates that the density region is smaller than $2n_0$ or larger than $5n_0$ and the thin line indicates the interpolated region. From the figure, for $m_0 = 800$ MeV,

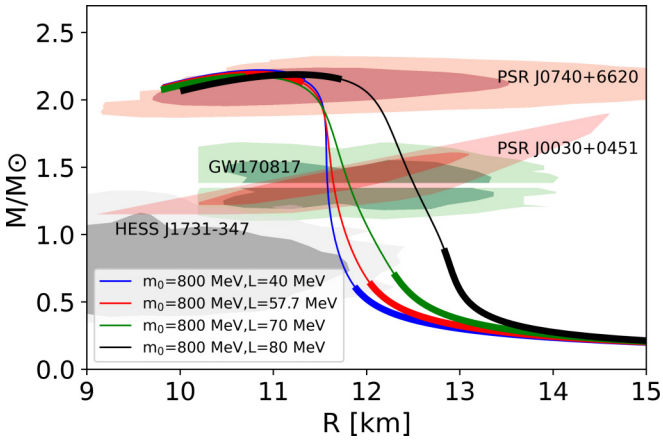

FIG. 4. Mass-radius relations for same $m_0 = 800$ MeV in different PDM sets. The black curve is connected to the NJL parameters $(H,\ g_V)/G = (1.5, 1)$, the green curve to $(H,\ g_V)/G = (1.55, 1)$, the red curve to $(H,\ g_V)/G = (1.55, 1)$, and the blue curve to $(H,\ g_V)/G = (1.55, 1)$.

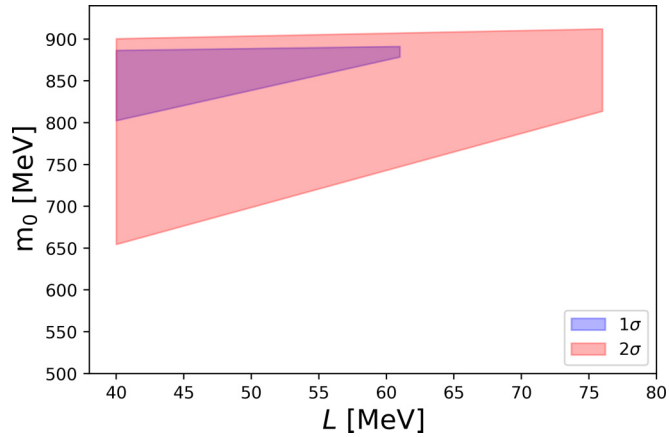

FIG. 5. Allowed region for m_0 and L. Within the shadowed region, the M-R curve satisfies all the constraints from the NS observation within the error of 1σ or 2σ.

the radius for $L = 40$ MeV, $M \simeq 1.4\ M_\odot$, is about 11.5 km, while the result of $L = 80$ MeV is about 12.6 km. This result indicates that EOSs are softened by the effect of the $\omega\rho$ interaction. One can see that the M-R curve for $L = 40$ MeV satisfies the constraint from the HESS J1731-347 observation. We note that $L = 40$ MeV is consistent with the one obtained in Ref. [50], due to a large ambiguity. Precise determination of the slope parameter in future will help us to further constrain the NS properties.

To achieve a NS with a small radius, the outer-core EOS (density around $1n_0$–$2n_0$) is extremely important, since it directly connects to the radius of a neutron star. In our model, the chiral invariant mass m_0 and the slope parameter L are two factors which have impacts on the outer-core EOS. We then treat them as free parameters and compare the corresponding M-R curves with NS constraints from NICER, gravitational wave detection, and HESS. We show the allowed region of m_0 and L satisfying all the observational constraints in the 1σ and 2σ range as in Fig. 5. Under this parameter space favoring large m_0 and small L, HESS J1731-347 can be considered as the lightest NS.

IV. SUMMARY AND DISCUSSIONS

In this study, we use parity doublet model together with the NJL-type model within the framework of the relativistic mean-field model to describe low-mass neutron stars. We construct the EOS for NS matter by interpolating the EOS obtained in the PDM and the one in the NJL-type model by assuming the crossover from hadronic matter to quark matter. In the calculation of the NS mass-radius relation, we find the outer-core EOS is crucial to determine the radius of a NS. Consequently, the choices of the chiral invariant mass m_0 and the slope parameter L which describe the properties of the uniform nuclear matter are essential. We treat m_0 and L as two free parameters and find the parameter space enables us to explain the HESS J1731-347 as a neutron star as in Fig. 5.

We note here that the typical estimate of L falls within the range of 40–80 MeV, as indicated by various studies [50,57,58]. However, there are also other estimates such as $L = (109 \pm 36.41)$ MeV derived from the analyses of neutron skin thickness from the PREX-2 experiment. There are still large ambiguities about the value of slope parameter. In the present research, we follow Ref. [50] as the baseline to set $L = 57.7 \pm 19$ MeV and study the corresponding mass-radius relation. If future experiments show the value of the slope parameter is large, we can come to the conclusion that HESS J1731-347 cannot be explained as a NS within the present model.

As studied in Refs. [13,59,60], the validity of pure hadronic descriptions at $n_B \geqslant 2n_0$ are questionable as nuclear many-body forces are very important, implying that quark descriptions are required even before the quark matter formation. In this study, we choose the interpolation point to be $2n_0$ and the ambiguity from the interpolation point is discussed in Fig. 6. In this figure, we show the M-R curves for $m_0 = 850$ MeV and $L = 40$ MeV with changing the interpolation range from $2n_0$–$5n_0$ to $1.5n_0$–$5n_0$ and $2.5n_0$–$5n_0$. We can easily

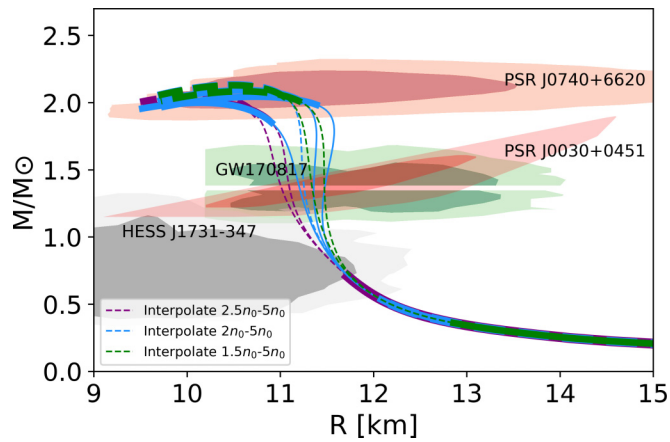

FIG. 6. Mass-radius relations for $m_0 = 850$ MeV and $L = 40$ MeV, and corresponding curves for central density. Different colors indicate different interpolation ranges.

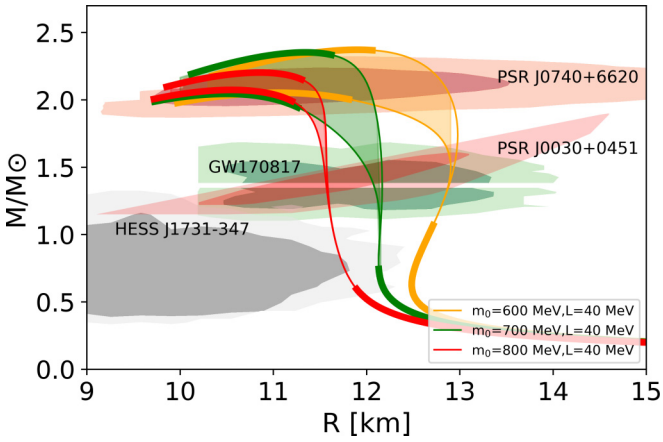

FIG. 7. Mass-radius relations for $m_0 = 600$, 700, and 800 MeV with $L = 40$ MeV. Orange curves are for $(H, g_V)/G = (1.55, 1.3)$ and $(1.45, 0.8)$; green curves are for $(H, g_V)/G = (1.6, 1.3)$ and $(1.5, 0.8)$; and red curves are for $(H, g_V)/G = (1.55, 1)$ and $(1.5, 0.8)$.

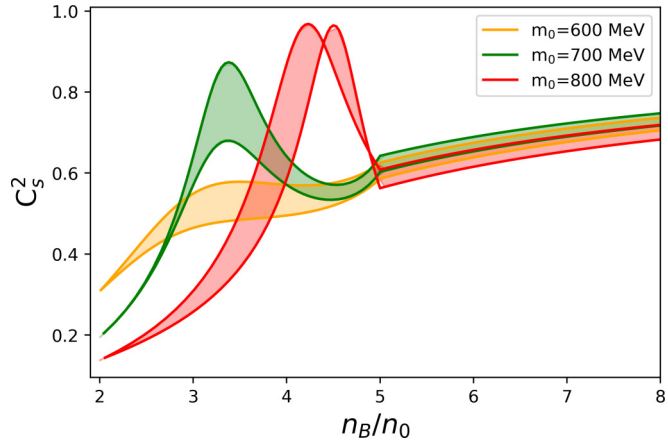

FIG. 8. Sound velocity for $m_0 = 600$, 700, and 800 MeV. The NJL parameters are the same as those in Fig. 7.

see that the ambiguity from the interpolation point is very limited: at the mass about 1 $M_\odot$, the radius shifts are only about 0.1 km.

In Fig. 7, we fix the value of the slope parameter as $L = 40$ MeV and vary the value of m_0 as $m_0 = 600$, 700, and 800 MeV. We choose the values of (H, g_V) parameters to produce the most stiff and the most soft EOSs satisfying the $2\,M_\odot$ constraint. For $m_0 = 700$ and 800 MeV, the rather soft hadronic EOSs are connected with rather stiff quark EOSs satisfying the $2\,M_\odot$ constraint, resulting in a peak of the density dependence of the sound velocity, as shown in Fig. 8. However, for $m_0 = 600$ MeV, the rather stiff hadronic EOS is used to connect with stiff quark EOSs, resulting in just a bumplike structure. Besides, we find that the onset density of the sound velocity peak is larger for larger m_0. Reference [61] pointed out that the appearance of the maximum in the speed of sound in the interior of NSs might indicate the change of medium composition, from hadronic to quark or quarkyonic matter. They estimate the critical density where baryons begin to overlap as $n_c^{\rm per} = 1.22/V_0$, $V_0 = (4/3)\pi R_0^3$ [62]. After using the experimental value of the proton radius $R_0 = 0.9 \pm 0.05$ fm [63,64], the critical density is calculated as $n_c^{\rm per} = 0.57^{+0.12}_{-0.09}$ fm^{-3}. When we require that the peak density of the sound velocity in the present analysis should satisfy $0.48 \leqslant n_B^{\rm peak} \leqslant 0.69$, i.e., $3 \leqslant n_B^{\rm peak}/n_0 \leqslant 4.3$, we obtain the constraint to the chiral invariant mass as $600 \lesssim m_0 \lesssim 800$ MeV for $L = 40$ MeV.

Finally, we note that in our current work we have focused on the scenario of a smooth crossover transition between hadronic and quark matter, as described by the interpolation between the PDM and NJL models. This choice is motivated by the fact that a crossover transition allows for a more gradual change in the EOS, which can be more easily reconciled with the observed properties of NSs, such as the LIGO-VIRGO and NICER events, which all have a similar radius for NSs. A strong first-order phase transition generally leads to a sudden change of the radius which is not favored by the observation constraints. In this case, we do not consider the first-order phase transition in this work.

ACKNOWLEDGMENTS

The work of B. Gao and M. Harada is supported in part by JSPS KAKENHI Grants No. 20K03927, No. 23H05439, and No. 24K07045. B. Gao is also supported by JST SPRING under Grant No. JPMJSP2125. B. Gao would like to take this opportunity to thank the Interdisciplinary Frontier Next-Generation Researcher Program of the Tokai Higher Education and Research System.

[1] B. P. Abbott *et al.* (LIGO Scientific Collaboration and Virgo Collaboration), GW170817: Observation of gravitational waves from a binary neutron star inspiral, Phys. Rev. Lett. **119**, 161101 (2017).

[2] B. P. Abbott *et al.*, Multi-messenger observations of a binary neutron star merger, Astrophys. J. Lett. **848**, L12 (2017).

[3] B. P. Abbott *et al.* (LIGO Scientific, Virgo), GW170817: Measurements of neutron star radii and equation of state, Phys. Rev. Lett. **121**, 161101 (2018).

[4] M. C. Miller *et al.*, The radius of PSR J0740+6620 from NICER and XMM-Newton data, Astrophys. J. Lett. **918**, L28 (2021).

[5] T. E. Riley *et al.*, A NICER view of the massive pulsar PSR J0740+6620 informed by radio timing and XMM-Newton spectroscopy, Astrophys. J. Lett. **918**, L27 (2021).

[6] S. Vinciguerra *et al.*, An updated mass–radius analysis of the 2017–2018 NICER data set of PSR J0030+0451, Astrophys. J. **961**, 62 (2024).

[7] V. Doroshenko, V. Suleimanov, G. Pühlhofer, and A. Santangelo, A strangely light neutron star within a supernova remnant, Nat. Astron. **6**, 1444 (2022).

[8] P.-C. Chu, X.-H. Li, H. Liu, M. Ju, and Y. Zhou, Properties of isospin asymmetric quark matter in quark stars, Phys. Rev. C **108**, 025808 (2023).

[9] P. T. Oikonomou and C. C. Moustakidis, Color-flavor locked quark stars in light of the compact object in the HESS J1731-347 and the GW190814 event, Phys. Rev. D **108**, 063010 (2023).
[10] T. E. Restrepo, C. Providência, and M. B. Pinto, Nonstrange quark stars within resummed QCD, Phys. Rev. D **107**, 114015 (2023).
[11] S.-H. Yang, C.-M. Pi, X.-P. Zheng, and F. Weber, Confronting strange stars with compact-star observations and new physics, Universe **9**, 202 (2023).
[12] I. A. Rather, G. Panotopoulos, and I. Lopes, Quark models and radial oscillations: Decoding the HESS J1731-347 compact object's equation of state, Eur. Phys. J. C **83**, 1065 (2023).
[13] G. Baym, T. Hatsuda, T. Kojo, P. D. Powell, Y. Song, and T. Takatsuka, From hadrons to quarks in neutron stars: A review, Rep. Prog. Phys. **81**, 056902 (2018).
[14] T. Minamikawa, T. Kojo, and M. Harada, Quark-hadron crossover equations of state for neutron stars: Constraining the chiral invariant mass in a parity doublet model, Phys. Rev. C **103**, 045205 (2021).
[15] T. Minamikawa, T. Kojo, and M. Harada, Chiral condensates for neutron stars in hadron-quark crossover: From a parity doublet nucleon model to a Nambu–Jona-Lasinio quark model, Phys. Rev. C **104**, 065201 (2021).
[16] B. Gao, T. Minamikawa, T. Kojo, and M. Harada, Impacts of the $U(1)_A$ anomaly on nuclear and neutron star equation of state based on a parity doublet model, Phys. Rev. C **106**, 065205 (2022).
[17] C. DeTar and T. Kunihiro, Linear sigma model with parity doubling, Phys. Rev. D **39**, 2805 (1989).
[18] D. Jido, M. Oka, and A. Hosaka, Chiral symmetry of baryons, Prog. Theor. Phys. **106**, 873 (2001).
[19] G. Aarts, C. Allton, S. Hands, B. Jäger, C. Praki, and J.-I. Skullerud, Nucleons and parity doubling across the deconfinement transition, Phys. Rev. D **92**, 014503 (2015).
[20] G. Aarts, C. Allton, D. De Boni, S. Hands, B. Jäger, C. Praki, and J.-I. Skullerud, Light baryons below and above the deconfinement transition: Medium effects and parity doubling, J. High Energy Phys. **06** (2017) 034.
[21] G. Aarts, C. Allton, D. De Boni, and B. Jäger, Hyperons in thermal QCD: A lattice view, Phys. Rev. D **99**, 074503 (2019).
[22] H. Nishihara and M. Harada, Extended Goldberger-Treiman relation in a three-flavor parity doublet model, Phys. Rev. D **92**, 054022 (2015).
[23] H.-X. Chen, V. Dmitrasinovic, and A. Hosaka, Baryon fields with $U_L(3) \times U_R(3)$ chiral symmetry: Axial currents of nucleons and hyperons, Phys. Rev. D **81**, 054002 (2010).
[24] H.-X. Chen, V. Dmitrasinovic, and A. Hosaka, Baryon fields with $U_L(3) \times U_R(3)$ chiral symmetry. III. Interactions with chiral $[(3, \bar{3}) \oplus (\bar{3}, 3)]$ spinless mesons, Phys. Rev. D **83**, 014015 (2011).
[25] H.-X. Chen, V. Dmitrasinovic, and A. Hosaka, Baryons with $U_L(3) \times U_R(3)$ chiral symmetry. IV. Interactions with chiral $(8, 1) \oplus (1, 8)$ vector and axial-vector mesons and anomalous magnetic moments, Phys. Rev. C **85**, 055205 (2012).
[26] T. Minamikawa, B. Gao, T. Kojo, and M. Harada, Parity doublet model for baryon octets: Diquark classifications and mass hierarchy based on the quark-line diagram, Phys. Rev. D **108**, 076017 (2023).
[27] B. Gao, T. Kojo, and M. Harada, Parity doublet model for baryon octets: Ground states saturated by good diquarks and the role of bad diquarks for excited states, arXiv:2403.18214.
[28] T. Hatsuda and M. Prakash, Parity doubling of the nucleon and first-order chiral transition in dense matter, Phys. Lett. B **224**, 11 (1989).
[29] D. Zschiesche, L. Tolos, J. Schaffner-Bielich, and R. D. Pisarski, Cold, dense nuclear matter in a SU(2) parity doublet model, Phys. Rev. C **75**, 055202 (2007).
[30] V. Dexheimer, S. Schramm, and D. Zschiesche, Nuclear matter and neutron stars in a parity doublet model, Phys. Rev. C **77**, 025803 (2008).
[31] C. Sasaki and I. Mishustin, Thermodynamics of dense hadronic matter in a parity doublet model, Phys. Rev. C **82**, 035204 (2010).
[32] C. Sasaki, H. K. Lee, W.-G. Paeng, and M. Rho, Conformal anomaly and the vector coupling in dense matter, Phys. Rev. D **84**, 034011 (2011).
[33] S. Gallas, F. Giacosa, and G. Pagliara, Nuclear matter within a dilatation-invariant parity doublet model: The role of the tetraquark at nonzero density, Nucl. Phys. A **872**, 13 (2011).
[34] J. Steinheimer, S. Schramm, and H. Stöcker, Hadronic SU(3) parity doublet model for dense matter and its extension to quarks and the strange equation of state, Phys. Rev. C **84**, 045208 (2011).
[35] W.-G. Paeng, H. K. Lee, M. Rho, and C. Sasaki, Dilaton-limit fixed point in hidden local symmetric parity doublet model, Phys. Rev. D **85**, 054022 (2012).
[36] V. Dexheimer, J. Steinheimer, R. Negreiros, and S. Schramm, Hybrid stars in an SU(3) parity doublet model, Phys. Rev. C **87**, 015804 (2013).
[37] W.-G. Paeng, H. K. Lee, M. Rho, and C. Sasaki, Interplay between ω-nucleon interaction and nucleon mass in dense baryonic matter, Phys. Rev. D **88**, 105019 (2013).
[38] A. Mukherjee, J. Steinheimer, and S. Schramm, Higher-order baryon number susceptibilities: Interplay between the chiral and the nuclear liquid-gas transitions, Phys. Rev. C **96**, 025205 (2017).
[39] D. Suenaga, Examination of $N^*(1535)$ as a probe to observe the partial restoration of chiral symmetry in nuclear matter, Phys. Rev. C **97**, 045203 (2018).
[40] Y. Takeda, Y. Kim, and M. Harada, Catalysis of partial chiral symmetry restoration by Δ matter, Phys. Rev. C **97**, 065202 (2018).
[41] H. Abuki, Y. Takeda, and M. Harada, Dual chiral density waves in nuclear matter, EPJ Web Conf. **192**, 00020 (2018).
[42] M. Marczenko, D. Blaschke, K. Redlich, and C. Sasaki, Parity doubling and the dense-matter phase diagram under constraints from multi-messenger astronomy, Universe **5**, 180 (2019).
[43] Y. Motohiro, Y. Kim, and M. Harada, Asymmetric nuclear matter in a parity doublet model with hidden local symmetry, Phys. Rev. C **92**, 025201 (2015).
[44] T. Yamazaki and M. Harada, Constraint to chiral invariant masses of nucleons from GW170817 in an extended parity doublet model, Phys. Rev. C **100**, 025205 (2019).
[45] A. Mukherjee, S. Schramm, J. Steinheimer, and V. Dexheimer, The application of the quark-hadron chiral parity-doublet model to neutron star matter, Astron. Astrophys. **608**, A110 (2017).
[46] M. Harada and T. Yamazaki, Charmed mesons in nuclear matter based on chiral effective models, in *Proceedings of the 8th International Conference on Quarks and Nuclear Physics*

(QNP2018), Tsukuba, Japan (The Physical Society of Japan, 2018).

[47] M. Marczenko, K. Redlich, and C. Sasaki, Chiral symmetry restoration and Δ matter formation in neutron stars, Phys. Rev. D **105**, 103009 (2022).

[48] T. Minamikawa, B. Gao, T. Kojo, and M. Harada, Chiral restoration of nucleons in neutron star matter: Studies based on a parity doublet model, Symmetry **15**, 745 (2023).

[49] Y. K. Kong, T. Minamikawa, and M. Harada, Neutron star matter based on a parity doublet model including the $a_0(980)$ meson, Phys. Rev. C **108**, 055206 (2023).

[50] B.-A. Li, B.-J. Cai, W.-J. Xie, and N.-B. Zhang, Progress in constraining nuclear symmetry energy using neutron star observables since GW170817, Universe **7**, 182 (2021).

[51] G. Baym, S. Furusawa, T. Hatsuda, T. Kojo, and H. Togashi, New neutron star equation of state with quark-hadron crossover, Astrophys. J. **885**, 42 (2019).

[52] T. Hatsuda and T. Kunihiro, QCD phenomenology based on a chiral effective Lagrangian, Phys. Rep. **247**, 221 (1994).

[53] R. C. Tolman, Static solutions of Einstein's field equations for spheres of fluid, Phys. Rev. **55**, 364 (1939).

[54] J. R. Oppenheimer and G. M. Volkoff, On massive neutron cores, Phys. Rev. **55**, 374 (1939).

[55] T. Kojo, QCD equations of state and speed of sound in neutron stars, AAPPS Bull. **31**, 11 (2021).

[56] G. Baym, C. Pethick, and P. Sutherland, The ground state of matter at high densities: Equation of state and stellar models, Astrophys. J. **170**, 299 (1971).

[57] C. Drischler, R. J. Furnstahl, J. A. Melendez, and D. R. Phillips, How well do we know the neutron-matter equation of state at the densities inside neutron stars? A Bayesian approach with correlated uncertainties, Phys. Rev. Lett. **125**, 202702 (2020).

[58] I. Tews, J. M. Lattimer, A. Ohnishi, and E. E. Kolomeitsev, Symmetry parameter constraints from a lower bound on neutron-matter energy, Astrophys. J. **848**, 105 (2017).

[59] K. Masuda, T. Hatsuda, and T. Takatsuka, Hadron-quark crossover and massive hybrid stars with strangeness, Astrophys. J. **764**, 12 (2013).

[60] K. Masuda, T. Hatsuda, and T. Takatsuka, Hadron–quark crossover and massive hybrid stars, Prog. Theor. Exp. Phys. **2013**, 073D01 (2013).

[61] M. Marczenko, L. McLerran, K. Redlich, and C. Sasaki, Reaching percolation and conformal limits in neutron stars, Phys. Rev. C **107**, 025802 (2023).

[62] P. Braun-Munzinger, A. Kalweit, K. Redlich, and J. Stachel, Confronting fluctuations of conserved charges in central nuclear collisions at the LHC with predictions from lattice QCD, Phys. Lett. B **747**, 292 (2015).

[63] B. Dey *et al.* (CLAS Collaboration), Data analysis techniques, differential cross sections, and spin density matrix elements for the reaction $\gamma p \to \phi p$, Phys. Rev. C **89**, 055208 (2014); **90**, 019901 (2014).

[64] T. Mibe, W. C. Chang, T. Nakano, D. S. Ahn, J. K. Ahn, H. Akimune, Y. Asano, S. Daté, H. Ejiri, H. Fujimura, M. Fujiwara, K. Hicks, T. Hotta, K. Imai, T. Ishikawa, T. Iwata, H. Kawai, Z. Y. Kim, K. Kino, H. Kohri *et al.*, (LEPS Collaboration), Near-threshold diffractive ϕ-meson photoproduction from the proton, Phys. Rev. Lett. **95**, 182001 (2005).